Micro displacement measured by the grating interferometer with rings pattern

A. Olivares-Perez
National Institute of Astrophysics, Optics and Electronics,
Street Luis Enrique Erro No. 1, Santa Maria Tonantzintla, Z.P. 72840, Puebla, Mexico,
Tel: 52 22 26 63 100
e-mail: olivares@inaoep.mx

Received 21 April 2014; accepted 19 September 2014

Micro displacements are measured with holographic gratings by using a grating interferometer of one order that detects the phase changes in the diffracted orders caused by movement of the grooves in the diffraction gratings. The period can be on the order of fractions of a micron, with high reproducibility and an error of a half period. The basic operating principle involves the superposition of order +1, with order 0. The interferometer system produces standing waves; it works by measuring the intensity variations at the center of a ring-shaped interference pattern, which indicate the phase shift introduced by displacement of the grating grooves. When these rings move to the center of the pattern or to the border, the direction of the grating displacement can be detected; the interferometer system has no moving parts, except for the diffraction grating, and is very stable and robust. This system has the ability to measure micro displacements even with damaged gratings, as long as the gratings diffract evenly.

Keywords: Diffraction gratings; grating interferometer; micrometer; displacement measurement.

PACS: 42.40.-I; 42.40.Eq; 42.40.Kw; 42.40.My

1. Introduction

We propose a concept for an opto-electronic system that is technically very simple and robust and that allows us to quantify micro- to nano-displacements. It works by measuring the intensity variations at the center of a ring-shaped interference pattern, which indicate the phase shift introduced by displacement of the diffraction grating.

The proposed system has the following main elements: a high quality diffraction grating, a source of laser light (diode) and a high-speed photodetector. The system is incorporated into a grating interferometer using only a diffracted order (-1) that detects the displacement of the grooves in the grating as phase shifts of the diffracted orders. The basic operating principle involves the superposition of the +1 order or -1 order diffracted by the grating, with the central order so as to produce standing waves. The system is very sensitive to the movement of the rows (grooves) of the grating.

The micrometer is common today, and it is used in various detection mechanisms, such as in the application of radiofrequency and optical signals [1], implementation in parallel optical planes with variable pitch [2], blocking parallel light beams to generate pulse signals [3], and measuring changes in absorption through absorber calibration [4]. On the other hand, diffraction gratings have been used to measure micro-movements with several techniques, such as: overlaying diffracted beams with orthogonal polarization [5]; photoelectric measurement to moving diffraction gratings [6]; displacement in the interference fringes produced by the diffraction of waves by a moving grating [7]; overlapping diffused light in a diffraction grating to detect changes in the visibility of the interference [8]; using diffraction gratings to measure micro-displacements by casting shadows [9]; by phase modulation effect of the diffracted orders, through Doppler effect, generated by a grating interferometer [10]; phase shifts by phase gratings with polarization modulation for multiple interferograms [11]; multiple orders interferometer produced by rotating gratings, phase shifts generated in multiple channels simultaneously [12]; with two diffraction gratings is generated an interferometer that detects the shift quadrature phase [13]; nano-displacement measurement with grating interferometer [14]; and following a preliminary work, where the proposed interferometer was published in proceedings of spie [15]. In this manuscript, we focus on the detection of the phase variations introduced by orders diffracted by a holographic grating by observing its Fourier spectrum [16-19].

The proposed interferometer has no moving parts, which makes it very sturdy and stable. The diffraction grating is the only moving part in the system; it can move in a linear or circular manner or by the rotation of a cylinder that is etched with the diffraction grating. The phase changes due to displacement of the grooves are detected by the proposed interferometer regardless of whether the diffraction grating is a transmission or reflection. We can measure the maximum and minimum intensity of the rings pattern, and the direction of grating movement to see if the rings pattern converges or diverges. When the rings are moved from the center of the ring to the edge, they diverge, and when the rings are moved from the edge to the center, they converge. This behavior is observed by moving the diffraction grating in one direction or another, perpendicular to the grooves. We have not seen a similar technique for measuring micro displacements in previously published papers; we observed significant advantages in the simplicity of the proposed interferometer presented here.

1.1. Micro-movements of diffraction gratings

One of the advantages of using diffraction gratings for measuring micro-displacements is the mechanical and thermal stability of the system compared to a conventional interferometer. The measuring accuracy of an interferometer is more direct and easy to measure. We can assume that diffraction gratings can be designed and fabricated with 1-micron periods in metric units (MU) (grating 1000 l/mm). Then, a micrometer detects the metric MU without any difficulties using an interferometer constructed with a grating and its diffracted orders. Furthermore, conventional interferometers are limited to integral multiples of the wavelength (mλ). This is not the same as the MU system where the wavelengths are derived from natural radiation depending on the characteristics of the light emitter.

We propose a system with only arbitrary wavelength and using only multiples of the periods of the diffraction grating (md), which can be designed in exact units in the metric MU system. Further, it can be scalable to the required precision. Gratings with: 1000, 2000, 4000, or 5000 lines/mm or more can be readily constructed.

However, with techniques such as the Michelson interferometer that, typically yield the highest resolution, an approximation is used because of the nature of the emission source that illuminates the interferometer, classical interferometers are naturally restricted by the wavelength. Furthermore, grating interferometers are independent of wavelength and depend only on the grating period, *i.e.* a single wavelength with several gratings may yield results with various accuracies. In conventional interferometers, it is necessary to change the laser or emitter source to increase accuracy.

2. Theory

2.1. Harmonic functions

We start from the basic principle of a grating of sinusoidal form $\sin(2\pi x/d)$, where the grating period is $d = 2\pi$. One

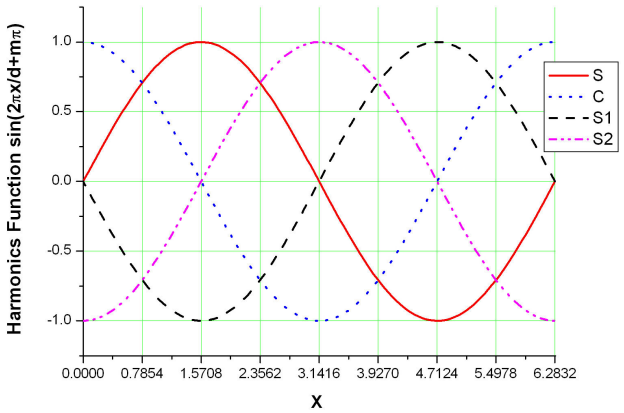

FIGURE 1. Graphs of $s = \sin(2\pi x/d)$ (solid line), $c = \cos(2\pi x/d)$ (dotted line), $s1 = \sin(2\pi x/d+\pi)$ (dashed line), and $s2 = \sin(2\pi x/d + 3\pi/2)$ (dashed dotted line). The behavior of the four functions is observed for a complete period $d = 2\pi$.

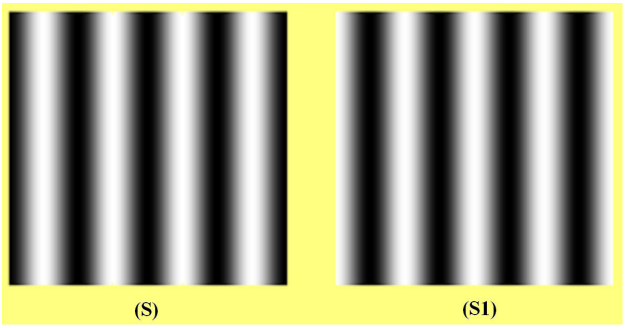

FIGURE 2. Two gratings with gray levels generated from: S and S1.

of the properties of this harmonic function, when it is implemented in a holographic grating, is that when it is moved by a factor of $d/4$, we obtain the function $\cos(2\pi x/d)$ [18,19]. Another important characteristic is that when we displace the grating by a factor of d/2, the result is similar to the sine function but with inverted amplitude values, which can be represented as $\sin(2\pi x/d + \pi)$. Furthermore a shift that inverts the cosine function is expressed by $\sin(2\pi x/d + 3\pi/2)$, as shown in Fig. 1.

The harmonic functions S and S1 are shifted by a factor of π, represented in the form:

$$S = \frac{1}{2} + \frac{1}{2}\sin\left(\frac{kx}{d}\right)$$
$$S1 = \frac{1}{2} + \frac{1}{2}\sin\left(\frac{kx}{d} + \pi\right) \qquad (1)$$

The functions S and S1 are generated for a numerical simulation, with gray levels from zero to 255. An offset of $d/2 = \pi$ between the two pattern fringes is clearly visible see Fig. 2. The features of these gratings correspond to amplitudes, so light diffraction would yield a very high intensity at the zeroth order and much lower intensity at the +1 and -1 diffracted orders.

2.2. Fourier transform

We used the Fourier transform and plotted the real part for the harmonic functions described in Sec. 2.1 (see Fig. 1) where one can observe a phase shift of $d/2 = \pi$. The diffracted orders are depicted in Fig. 3 [20-22], where the graphs of sf and $s1f$ correspond to the Fourier transforms of the functions S and $S1$ represented by Figs. 2. The functions S and $S1$ have a phase difference of $d/2$. For orders -1 and +1, the function sf and $s1f$ have positive and negative values, respectively, as shown in Fig. 3.

The result shown in Fig. 4 indicates phase changes due to displacement of the grating, which can be detected only by an interferometer like that proposed in Fig. 5. It is not possible to detect this variation in intensity; however, the interferometer was able to detect these phase variations.

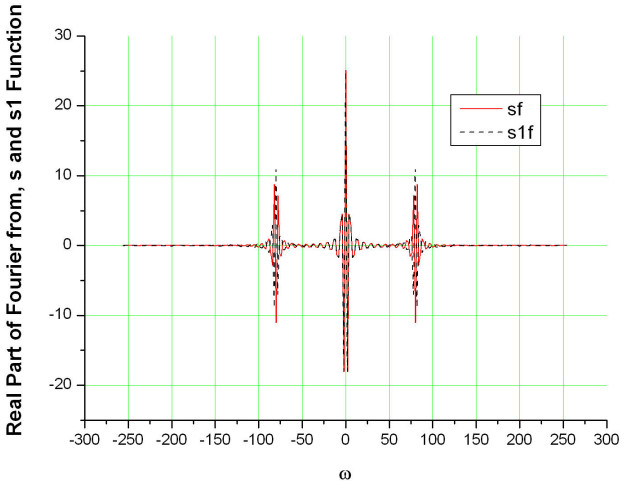

FIGURE 3. Real part of Fourier spectra, for sine functions sf (solid line) and $s1f$ (dashed line). This affords a raster phase when the grating is displaced by a factor of $d/2$.

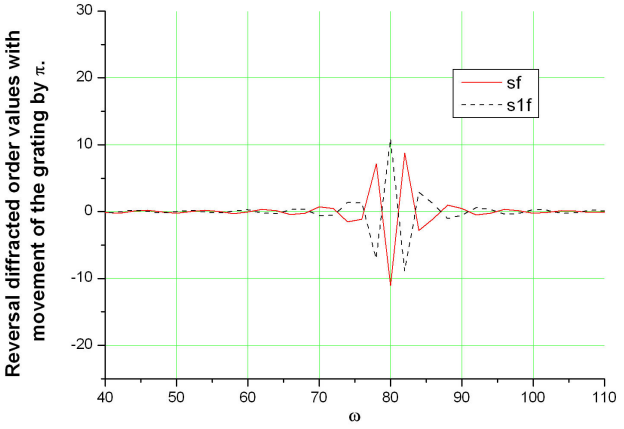

FIGURE 4. Reversal of diffracted order values (+1) upon movement of the grating period by $d/2$.

2.3. Phase Gratings

The complex transmittance of a sinusoidal phase grating can be expressed as:

$$t(x) = \exp\left[ia\cos\left(\frac{2\pi}{d}(x-x_0)\right)\right] \tag{2}$$

Where a, d, and x_0 are the amplitude phase modulation, period, and displacement from the origin along the x direction of the phase grating, respectively. Defining $\sigma(x_0) = 2\pi x_0/d$, and using Bessel function properties [23]:

$$\cos\left[a\cos\left(\frac{2\pi}{d}(x-x_0)\right)\right] = J_0(a) + 2\sum_{m=1}^{\infty}(-1)^m J_{2m}(a) \times \cos\left[2m\left(\frac{2\pi x}{d}+\sigma(x_0)+\frac{\pi}{2}\right)\right] \tag{3}$$

$$\sin\left[a\cos\left(\frac{2\pi}{d}(x-x_0)\right)\right] = 2\sum_{m=0}^{\infty}(-1)^m J_{2m+1}(a) \times \cos\left[[2m+1]\left(\frac{2\pi x}{d}+\sigma(x_0)+\frac{\pi}{2}\right)\right] \tag{4}$$

Using the Euler expression $\exp i(\theta) = \cos(\theta) + i\sin(\theta)$, with $\theta = a\cos((2\pi/d)(x-x_0))$, we can rewrite Eq. 1 in the form:

$$t(x) = \sum_{m=0}^{\infty} -i^m J_m(a)\cos\left[m\left(\frac{2\pi x}{d}+\sigma(x_0)+\frac{\pi}{2}\right)\right] \tag{5}$$

where $J_m(a)$ is the mth order Bessel function of the first kind. Using the identity $J_{-m}(a) = (-1)^m J_m(a)$, the relative phase of the mth diffracted order with respect to the zeroth order is given by [13]:

$$\varphi(x_0) = \begin{cases} m\left[\sigma(x_0)+\frac{\pi}{2}\right], & m \geq 1 \\ |m|\left[-\sigma(x_0)+\frac{\pi}{2}\right], & m \leq 1 \end{cases} \tag{6}$$

for a phase grating with a sinusoidal profile.

With Eq. 4, we can see that when m=1 and $x = \sigma(x_0) = 0$, we obtain, $-iJ_1(a)$, and for $x = \sigma(x_0) = \pi$, we obtain, $+iJ_1(a)$. The change of sign is predicted by the simulation in Fig. 4. The reversal of diffracted order (+1) shown in Fig. 4 is produced when the grating period is shifted by $\sigma(x_0) = d/2$. Only these phase changes can be detected by an interferometer [24].

3. Experimental Results

3.1. Setup of Grating Interferometer with Rings Pattern

The diffraction orders were generated with holographic gratings, but they can also be constructed mechanically. We built an interferometer in which +1 or -1 orders overlap with the zeroth order. As seen in Figs. 5(a) and (b), this produces standing waves. A lens is used after the laser beam output, causing the beam to diverge with a given radius of curvature because the interferometer arms are not placed at equal distances. That is, the distance between the grating and the output of the cube beam splitter (CBS) is slightly different between the path of the zeroth order and -1 order. This causes the ordinarily concentric rings to overlap. The zeroth order is usually the most intense but is attenuated with a neutral filter. The diffracted order for angles greater than 70 has an astigmatic deformation, *i.e.*, the diffracted order has an elliptical shape. To correct this anomaly, we recommend using a cylindrical lens. The lens that opens the laser beam has a diameter of 1 cm and a focal length of 1m, the cylindrical lens (CL) has a diameter of 1 cm and a focal length of 1 m. The behavior of this interferometer is similar to a Michelson or Twyman-Green, with mirrors M1, M2, M3, and M4; however, in this arrangement the positions of the mirrors do not vary with respect to the cube beam splitter, and only diffraction grating

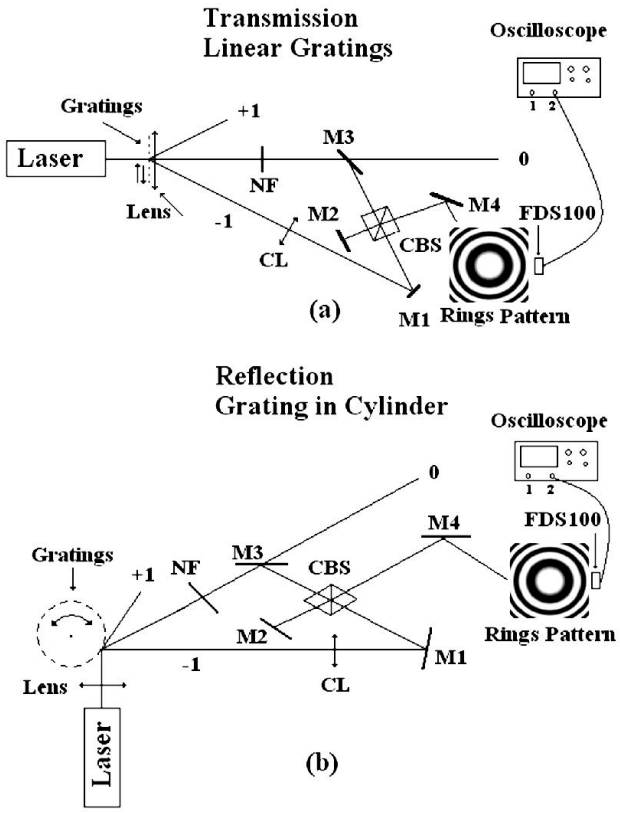

FIGURE 5. Two experimental arrangements used to measure micro movements of the grating. (a) Linear transmission grating [15]. (b) Reflection grating engraved on a cylinder which can be rotated to the right or left. M: mirror; CBS: cube beam splitter; NF: neutral filter; CL: cylindrical lens (optional).

grooves are displaced to the left or right. The system can be implemented using transmission gratings or reflection gratings, with the latter yielding more robust performance. Its ability to measure can be enhanced by fabricating the diffraction grating on a cylinder that rotates to the right or left. The system can measure displacement regardless of the physical size of the grating, as shown by the grating on the cylinder in Fig. 5(b).

When the -1 order overlaps the zeroth order (Fig. 5), we note a clear zone surrounding the ring center, which corresponds to the maximum, whereas the dark center of the ring corresponds to a minimum. Between the maximum and minimum displacement is a holographic grating of $d/2 = \pi$. Figure 6 shows the concentric ring patterns obtained by the arrangement in Fig. 5(a) with 1000 lines/mm, with $d = 1$ μm (grating #2, Table II). The behavior of these rings is peculiar in that they converge if the grating is shifted to the right and diverge if the grating is moved to the left, that is, when we superimpose orders -1 and 0. Moreover, the opposite behavior occurs when we superimpose orders +1 and 0; that is, the rings diverge if the grating is shifted to the right and converge if the grating is moved to the left. All the figures are illustrative, to show the idea, the figures shown in this manuscript are not the exact dimensions as for a design of a device.

This behavior is also important because it indicates the direction of movement of the diffraction grating. Figure 6 shows the half period shift $d/2 = \pi$. This can be quantified in terms of the distance between the dark center of the ring pattern and the next bright centered ring pattern by counting the maximum and minimum numbers of measured displacements of the grating (linear) or rotations (cylinder).

By counting the number of rings (counting variations of maximum and minimum in the center of the rings) with a high speed photo sensor, we can measure physical movements of the diffraction grating, which can be easily mounted on a precision mechanical device.

To get the rings pattern is very criticizes the system alienation, with a small error of alienation cannot be produced the rings pattern. The basic to align the system, the experimental procedure is to work without lenses (laser output and CL) in accordance with Fig. 5, They just have to superimpose the light spots observed through the cube beam splitter (CBS) reflected by the mirror M4. When a single point is observed, the system is aligned. Then the lenses can be then added. If the rings are distorted by astigmatism, then it is advisable to use the cylindrical lens CL. this lens is optional if the deformation is smaller.

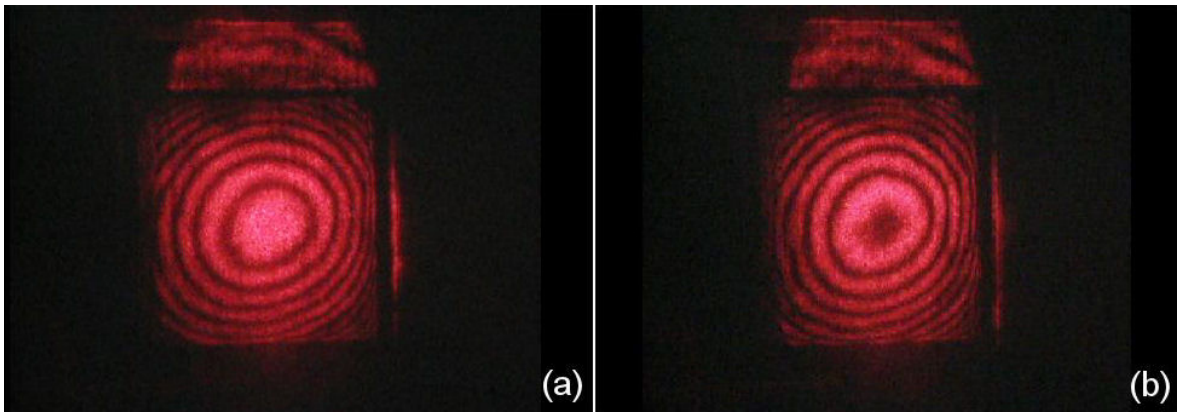

FIGURE 6. a) Maximum at the center of the ring groove determining the position of the grating. b) Minimum displacement, which corresponds to $d/2 = \pi$ of the grating with respect to image (a).

TABLE I. Parameters holographic gratings made in the laboratory.

Wavelength λ	X (mm)	Y(mm)	Θ (deg)	f(lines/mm)	d (mμ)	η(%)
	$\pm$ 0.5 mm	$\pm$ 0.5 mm	$\pm$ 0.05 deg	$\pm$ 2.5	$\pm$ 0.005 mμ	$\pm$ 0.5 %
Grating # 1						
$\lambda = 633$ nm	510	141	15.17	826.9	1.209	20.3
$\lambda = 604$ nm	510	134	14.45	826.3	1.210	10.3
$\lambda = 594$ nm	510	132	14.24	828.4	1.207	18.8
$\lambda = 543$ nm	510	120	12.99	828.2	1.207	28.5
(average)				827.5	1.208	
Grating # 2						
$\lambda = 633$ nm	510	173	18.40	997.5	1.002	18.1
$\lambda = 604$ nm	510	165	17.60	1001.2	0.998	8.8
$\lambda = 594$ nm	510	162	17.30	1001.1	0.998	13.0
$\lambda = 543$ nm	510	147	15.78	1002.2	0.997	14.0
(average)				1000.5	0.999	
Grating # 3						
$\lambda = 633$ nm	510	243	25.04	1338.1	0.747	16.2
$\lambda = 604$ nm	510	230	23.86	1339.1	0.746	6.6
$\lambda = 594$ nm	510	225	23.39	1337.2	0.747	6.7
$\lambda = 543$ nm	510	203	21.32	1339.1	0.746	6.7
(average)				1338.4	0.747	

3.2. Construction and characterization of holographic gratings

To check the operation of the interferometer in Fig. 5(a), we made three holographic gratings with different periods to demonstrate that, in fact, the movement of the grooves of the gratings is related to the movement of the rings in the interferometer. In Table I, the parameters of the gratings used are shown. We use a He-Ne tunable laser (Research Electro-Optics®) with 4 wavelengths in order to have more certainty in measuring the gratings period. Table I shows the X parameter, which corresponds to the distance between the grating and the screen that projects the diffracted orders. The Y parameter corresponds to the distance between the zeroth order and the +1 or -1 order; and θ is the angle formed between the -1 order diffracted beam and the zeroth order. Spatial frequency, f, of the gratings (lines/mm) was calculated using the Bragg equation; d is the inverse of the frequency in microns; and η corresponds to the diffraction efficiency of gratings reconstructed for each used wavelength.

The measured distances between the diffraction grating and the screen, parameter X, and the diffracted orders, parameter Y, are critical. In the laboratory, they measure in units of mm with an error of $\pm$ 0.5 mm, to calculate some differences in frequencies and periods due to the magnitude of the error. However, to reduce these discrepancies with these four measurements, for each grating we can get an average of the frequency and period of the gratings, which we use in our calculations. The angle θ was calculated numerically as $= a\tan(Y/X) * 180/\pi$, with an accuracy of $\pm$ 0.05 deg. This uncertainty is introduced by the error propagation of parameters X and Y. In the case of spatial frequency f, the corresponding error is $\pm$ 2.5 lines (fringes) per number of lines calculated with the angle θ using the Bragg equation. That is, if we calculate 1000 lines/mm we have an error of 2.5 lines, corresponding to 997.5 lines/mm or 1002.5 lines/mm per calculation, which is quite acceptable. The diffraction efficiency η, as expected, is different for each wavelength and corresponds to the sum of the intensities of the orders $\pm$ 1, divided by the incident beam intensity Ii, per one hundred; that is $\eta = (I_{\pm 1}/I_i) \times 100$, with an error of ± 0.5 %.

The twisting effect is feasible if the grating is built with a soft material, generally a glass substrate is used for remove this problem.

3.3. Grating interferometer with overlap orders vs. grating interferometer with rings pattern

To determine the relationship between the phase changes generated by the movement of the gratings and the rings generated by the setup of Fig. 5(a). We use the schemes described in Figs. 7 and 9 with overlapping orders, and amplification and gratings respectively. The gratings 1, 2 and 3 described in Table I, could be visualized with an amplifying power of 60x (Edmund®). The intensity of the projected fringes was measured by two sensors (Silicon Photodiode

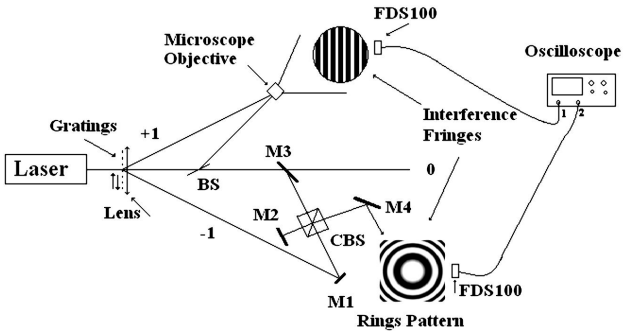

FIGURE 7. Diagram comparing the phase changes introduced by the grating in motion, grating interferometer with overlap orders, channel 1; grating interferometer with rings pattern, channel 2, of the oscilloscope.

FDS100®). We measured intensity variations by moving the fringes generated by the grating interferometer with overlap orders, and by the interferometer with rings pattern as shown in Fig. 5(a). In this figure, the oscilloscope channel 1 corresponds to the information reading obtained with overlapping +1 and 0 orders, and channel 2 corresponds to a standing waves interferometer with the reading obtained by overlapping -1 and 0 orders, showing that both channels have similar behavior in the detection of signals (see Fig. 7). Measurements were made for the three gratings described in Table I. Figure 7 illustrates the scheme used to obtain the results of the two interferometers.

Both interferometers detect the same intensity distribution variation within their respective scales for the holographic gratings in motion. This is consistent with the theory outlined in Sec. 2. A point to note is that both interferometers have the same sensitivity for detecting phase changes introduced by the gratings in motion. However, it is much more practical to display fringes with the standing wave interferometer in Fig. 5(a) because only a low-power single lens is needed to generate spherical wavefronts sufficient for visualizing the rings. Furthermore, the interferometer constructed by overlapping the +1 and zeroth orders, reflected by the BS, is about 20 degrees (see Fig. 7), they requires a microscope objective of 60x or higher power, which greatly reduces the intensity owing to the cone of light emerging from the 60x objective and the inherent noise it produces that overlaps with the fringe pattern. The distance of the microscope objective to the magnified image with the interference fringes (lines) was 2 m; the image diameter was 60 cm. On the other hand the rings diameter was the order of 1 cm.

In Fig. 8 measured signals of 3 gratings, are shown from lowest frequency gratings to higher frequency gratings. The grating of 1000 l/mm was used to build the interferometer that displayed the rings in Figs. 6 and 8.

3.4. Detecting phase changes by both interferometers

Figure 8 shows the results obtained from the setup described in Fig. 7 for the three gratings. Figure 8 (a), (b) and (c) correspond to gratings 1, 2, and 3, respectively. The upper signals correspond to the grating period, and the lower signals correspond to rings period of the oscilloscope. Upper signals in Figs. 8(a), (b), and (c) represent the phase changes of the grating interferometer with overlap orders, which is generated by superimposing the +1 order and the zeroth order. The photosensor (FDS100®) detects the maximum and minimum variation of the projected fringes, which are displayed on the oscilloscope as a harmonic signal. The lower signals in Figs. 10(a), (b) and (c) represent phase changes of the grating interferometer with standing waves forming the rings pattern shown in Fig. 5(a), which is generated by superimposing the -1 order and the zeroth order. The fringes produced by this interferometer, move when the grating is shifted, and the photo sensor detects the maximum and minimum variation of the rings, which are displayed on the oscilloscope as a harmonic signal.

In all gratings Fig. 8 shows that the phase variations detected by both interferometers are the same. This is demonstrated by counting the number of crests of the harmonic functions for upper and lower signals of Fig. 8. Except for slight phase shifts, this is due primarily to the physical positioning of the photo sensor on the fringes. To ensure that both channels were in phase, the photo sensor was located in a dark fringe for both signals. A significant problem in this setup is the noise introduced when the beam is expanded with

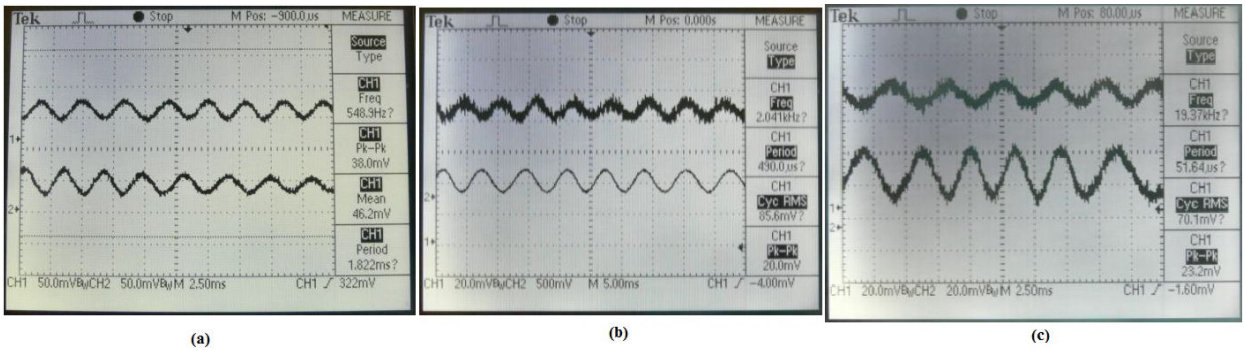

FIGURE 8. Comparison of the phase changes by grating movement generated by the grating interferometer with overlap orders (upper signal) and the grating interferometer with rings pattern (lower signal) with (a) grating 1, (b) grating 2, and (c) grating 3.

microscope objectives of 60x and 100x for the grating interferometer. This noise signal overlaps with the fringes making the correct location difficult to pinpoint. As can be seen in Fig. 8(b), the information from upper signal is more diffuse due to the lighting generated by the noise that was introduced to expand the beam, and by small defects in the substrate of the grating. This noise effect was prevalent when increasing the voltage amplitude in the signal at the oscilloscope. Conversely, there is no such problem in detecting the fringes for lower signal. In Fig. 8(c) both signals were scaled to display additional voltage signals because of similar noise problems as seen in the 8(b) grating. Figures 8(a), (b), and (c) clearly show that the phase variations introduced by the movement of the gratings are the same for the grating interferometer with overlap orders and for the grating interferometer with rings pattern.

Clearly, the grating interferometer with rings pattern is much more robust than the grating interferometer with overlap orders. Specifically, with the grating interferometer with rings pattern, only with a simple low power lens is required to display the rings. Moreover, the photosensor area is not critical for measuring the intensity of the rings. By contrast, this area is very important when trying to measure the intensity of the fringes projected by the conventional grating interferometer with overlap orders. In this latter case, it is crucial that the photosensor area be lower than the projected fringes period in order to measure the intensity variations as shown in Fig. 8. The photosensor area is of 2 mm^2; the period of the fringes was approximately 2.5 mm. On rings, the photosensor is in the centre of the rings pattern, which changes from maximum to minimum when the grating is moved regardless of the period of the rings.

3.5. Grating period vs. phase shift due to displacement

Figure 9 shows the experimental setup used to measure the displacements of the grating grooves with respect to the phase change, detected by the grating interferometer with rings pattern. In principle, when the grating is enlarged (grating 2) along with its projected image using a 100x microscope objective noise is introduced by the microscope objective (internal lenses, rayons, and dust, for example.). Noise may also be introduced by small variations of uniformity of the substrate material where the grating is recorded. The noise is then superimposed on the projected fringes (typically low contrast) that correspond to the grooves of the amplified grating. This is detected by a photosensor (FDS100®), which ensures that the area of the photosensor is less than the space between the projected fringes. This information was detected on upper signal of Fig. 10. However, the generated ring by the grating interferometer of standing waves described in Figure 5 does not have these drawbacks, because the amplification is minimal with very good signal reception and the interferometer forms fringes of rings with very good contrast. The signal for this interferometer is detected by the photosensor on, lower signal (Fig. 10). it is clear that, the angle between the zero order and the +1 is about 30 degrees, the cylindrical lens in this case is not necessary, so in Figs. 7 and 9 is not shown.

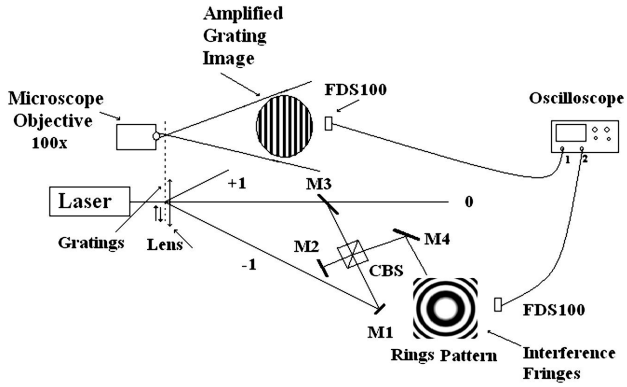

FIGURE 9. Experimental setup for detecting the grating grooves channel 1 and the phase shifts introduced by displacement of the grating, detected by grating interferometer with rings pattern channel 2.

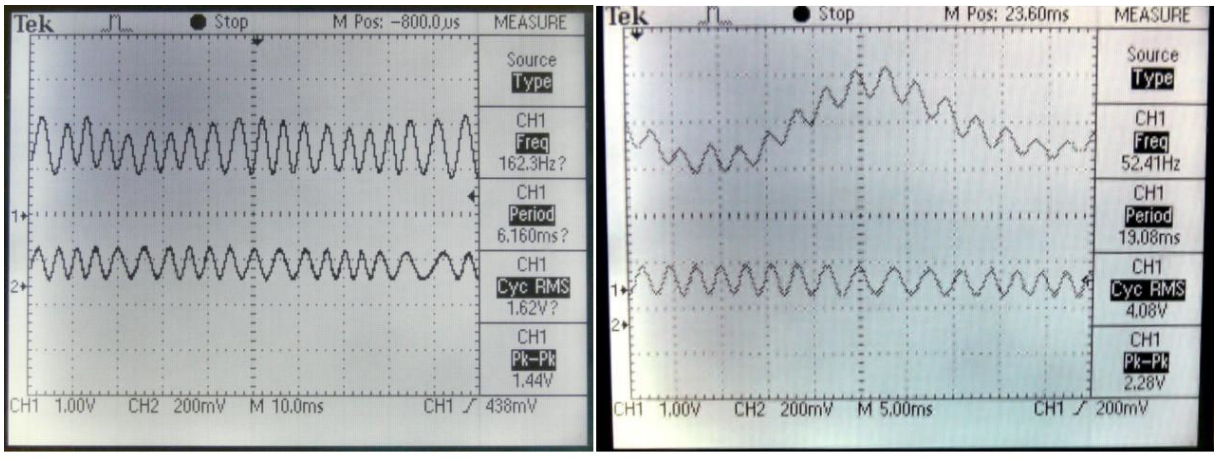

(a) (b)

FIGURE 10. Measurements obtained from the setup of Fig. 9, where the upper signal corresponds to grating period, and the lower signal to rings period. (a) displacement measurement one, (b) displacement measurement two.

Figure 10 shows the results obtained by the experimental setup of Fig. 9. On upper signal, the signals vary in amplitude and smaller phase shifts, due to overlapping of noise inherent in the experiment. However, in lower signal there are no variations in amplitude, and the signal is much clearer. The results demonstrate that there is a correspondence between the grating grooves and the phase shift introduced by the grating displacement, which is supported by the theory outlined in Sec. 2. These measurements were performed with grating 2. From the results shown in Figs. 10(a) and (b), we can quantify the physical displacement in a portion of the sampling time. There are 19 spaces between the peaks in Fig. 10(a), which correspond to approximately 19 microns of displacement. In Fig. 10(b) there are 16 spaces, which correspond to 16 microns of displacement.

The upper signals in Fig. 10 are clearer than those shown in Figs. 9 and 11. This is because the use of a 100x oil immersion microscope objective (Edmund®), with a diameter of 3 mm, which provides more energy and amplification. In Figs. 9 and 11, the results were obtained with a microscope objective of 60x with 2 mm diameter, with lower intensity and lower amplification. Therefore, the distance from the photosensor and the grating was greater, producing increased noise and resulting in a low contrast in the projected fringes.

3.5.1. Measurement of displacement, with damaged gratings

One problem with using gratings is that they may suffer wear and tear and have embedded noise in the substrate, due to such things as scratches or dirt. However, if the grating diffracts properly, it is sufficient for measuring displacements of the grating interferometer with rings pattern (Fig. 5). These measurements were made with gratings (Edmund®) in a substrate of acetate with 1000 l/mm (old and battered by use). Using a microscope objective of 60x, and noting the details of Fig. 11, we can quantify the physical displacement in a portion of the sampling time. We count 7 spaces between the peaks, which corresponds to about 7 microns of displacement.

The results reaffirm the instrument's capacity, which reinforces our proposed grating interferometer with rings pattern (Fig. 5). In all experimental measurements, the signal obtained by the oscilloscope on lower signal (channel 2), in the schemes of Figs. 5, 7 and 9, was the best. This clearly demonstrates the improved efficiency of measuring grating displacements using this technique. One advantage of this technique is the robustness of the system to measure with diffraction grating damaged. This is shown in Fig. 11.

3.6. Measurements

Measurements made with the diffraction grating 2 and a mechanical micrometer newport, Model 425 of linear precision. Table II shows the accuracy of the proposed system Fig. 5(a), noting, that the read error newport mechanical micrometer 425 is of $\pm$ 5 μm. Furthermore the proposed system has a read error $\pm$ 5 μm. The accuracy of the proposed system is 10 times more. The procedure for obtaining the data in Table II, was to displace the grating 2 with mechanical micrometer. We measured with the graduated lines of the vernier from micrometer newport 425. Moreover, with the photosen-

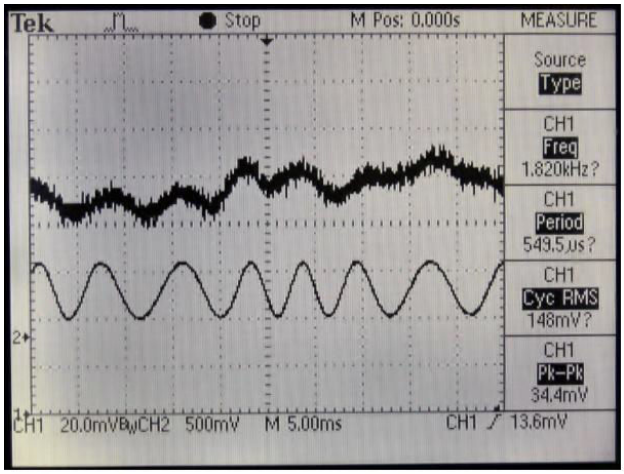

FIGURE 11. Measurements obtained from the setup of Fig. 9, with damaged gratings (grating with high noise). The upper signal corresponds to grating period, and the lower signal to rings period.

TABLE II. Compare measurements with a mechanical displacement interferometer Newport, and the proposed interferometer with the grating 2.

Mechanical Micrometer Newport Micrometer N Lines (10 μm per line)	Mechanical Micrometer Newport Micrometer Displacement ($\pm$ 5 μm)	Grating # 2 Grating Interferometer N Rings (1 μm per ring, d)	Grating # 2 Grating Interferometer Displacement ($\pm$ 0.5 μm, $d/2$)
5	50	51	51
12	120	119	119
27	270	271	271
38	380	378	378
45	450	451	451
78	780	778	778
93	930	931	931

sor (FDS100®), the number of rings (N) generated by shifting the grating were counted.

4. Discussion and conclusions

A key feature of the proposed system is its robustness. The physical diffraction grating can be constructed from a polymer and can be modulated by relief, refractive index or amplitude. A low thermal expansion polymer can be used. The grating can be read by transmission or reflection. What is important is whether the +1 or -1 order diffraction grating overlaps with the zeroth order.

The interferometer moves the grooves or the periods of the grating, and whether the rings converge or diverge depends on the direction of the displacement of the grating. The maximum to maximum detected in the rings are related to the grating period $d = 2\pi$. Our proposal is based on multiples and submultiples of the periods of the diffraction grating (md). It can also be scaled to the precision needed. Diffraction gratings with 1000, 2000, 4000, or 5000 lines/mm or more can be readily constructed. The maximum and minimum values of ring pattern intensity are easily measured, so the interval between those two measurements would be $d/2 = \pi$ and would correspond to the measurement uncertainty. That is, in a grating of 1000 lines/mm, the period would be $d = 1\ \mu$m $\pm$ 0.5 μm, which is quite acceptable.

Figure 5 is an experimental scheme to produce standing waves in the form of rings. These allow for more easily measured intensity variations that are independent of the photosensor area. The proposed instrument demonstrates the ability to measure the phase changes introduced by the motion of the gratings. The data obtained with the channel 2 of oscilloscope showed more uniformity and clarity, and the robustness of this proposed instrument was demonstrated when phase changes could be measured using damaged gratings. Other research relating to grating interferometers, does not appear to investigate measurements with damaged gratings. We demonstrated that the grating interferometer with overlap orders and the grating interferometer with rings pattern both detect the same phase changes, introduced by the motion of the gratings. Furthermore, we demonstrated experimentally that there is a clear correspondence between the displacement of the grooves and the detected phase changes, *i.e.*, when a groove is shifted half a period $d/2 = \pi$. Finally, another important finding is the robustness of the system in detecting phase shift information, despite the noise that may be implicit in the diffraction grating due to such things as structural defects, damage from wear and tear, misuse, or scratches.

The geometry to produce standing waves with the grating interferometer is very similar to that of the Michelson or Twyman-Green interferometers, with an accuracy of $\lambda/2 \pm \lambda/4$, while the grating interferometer has an accuracy of $d \pm d/2$. While the Michelson interferometer by its nature is more accurate, the grating interferometers is scalable by changing the grating, and since grating interferometers are independent of wavelength, we can easily achieve various accuracies. In conventional interferometers, it is necessary to change the laser or emitter source to increase accuracy.

To get high robustness in the system, the entire interferometer can be isolated adiabatically to give it more thermal and mechanical stability or protection against corrosive elements. The only moving part is the grating itself.

Acknowledgments

We thank Mr. Chemist Israel Fuentes, for his support with the experimental results and for the preparation of the holographic gratings, which strengthened our research, and the permission of the editorial office of SPIE for Fig. 5(a).

1. D. G. Heflinger and L. O. Heflinger, *US Patent* 6243168 B1, 5 June (2001).
2. T. J. Rolbiecki and D. L. Sanders, *US Patent* 5414646 A, 9 May (1995).
3. B. Richter and B. Brand , *US Patent* 4492473, 1 August (1985).
4. S. H Jones, C. DeMain, R. A Ross, D. Abdallah, and T. Digges, *US Patent* 5754294, 19 May (1998).
5. K. Ishizuka and T. Nishimura, *US Patent* 5436724 A, 25 July (1995).
6. E. Leitz, *UK Patent* GB1439645(A), 16 June (1976).
7. C. Kabushiki-Kaisha (Tokyo, JA), *US Patent* 3836257, 17 September (1974).
8. A. Kuroda (Tokyo, JP), *US Patent* 20120257214, 10 November (2012).
9. M. R. Gomez-Colin, A. Olivares-Pérez, and V. Sénchez-Villicaña, in Proceedings Practical Holography XV and Holographic Materials VII, 2001, edited by Stephen A. Benton, Sylvia H. Stevenson, T. John Trout, (SPIE-The International Society for Optical Engineering, San Jose California USA, 2001) 4296, p. 108.
10. F. Kuang-Chao, L. Yu-Sheng, C.Ye-Jin, and C. Fang, in Proceedings *Third International Sym. on Precision Mechanical Measurements*, edited by Fan Kuang-Chao, Wei Gao, Xiaofen Yu, Wenhao Huang, Penghao Hu, (SPIE-The International Society for Optical Engineering, Urumqi, China, 2006), 6280, p. 628008-1.
11. G. Rodriguez-Zurita, C. Meneses-Fabian, Noel-Ivan Toto-Arellano, J. F. Vázquez-Castillo, and C. Robledo-Sánchez, *Opt. Exp.* **16** (2008) 7806.
12. J. Howard, *Appl. Opt.* **31** (1992) 1419.
13. Y. Zahid, W. Jigang, C. Xiquan, H. Xin, and Y. Changhuei, *Opt. Exp.* **14** (2006) 8127.

14. J. Minlan, L. Fupeng, W. Xiaodong, *App. Mech. and Mat.* **103** (2012) 35.

15. A. Olivares-Pérez, M. Alejandra Lara-Peña, J. A. García-Monge, P. A. Valencia-Acuña, J. M. Villa-Hernández, and I. Fuentes-Tapia, in Proceedings *Practical Holography XXVII: Materials and Applications*, 2013, edited by Hans I. Bjelkhagen, V. Michael Bove, Jr., (SPIE-The International Society for Optical Engineering, San Francisco USA, 2013) 8644, p. 864415-1.

16. J. Collier, C. B. Burckhardt, and L. H. Lin, *Optical Holography* (Academic Press, New York, USA, 1971) p. 266.

17. E. N. Leith and J. Upatnieks, *J. Opt. Soc. Am.* **52** (1962) 987.

18. M. Hazewinkel, Periodic function, *Encyclopedia of Mathematics* (Springer, ISBN 978-1-55608-010-4, 2001).

19. K. Knopp, *Periodic Functions* (Dover, 1996). pp. 58-92.

20. J. Spanier and K. B. Oldham, *Periodic Functions* (Hemisphere, 1987). pp. 343-349.

21. E. M. Stein and G. Weiss, *Introduction to Fourier Analysis on Euclidean Spaces* (Princeton University Press, ISBN 0-691-08078-X, 1971).

22. K. B. Howell, *Principles of Analysis* (CRC Press. ISBN 978-0-8493-8275-8, 2001).

23. M. Abramowitz, and I. A. Stegun, *Handbook of Mathematical Functions* (Dover Publications Inc., New York USA, 1972) pp. 360-361.

24. D. Malacara, *Óptica Básica* (Fondo de Cultura Económica, USA, ISBN-13: 9789681673130 2004).